Eur. Phys. J. B **5**, 379–388 (1998)

THE EUROPEAN PHYSICAL JOURNAL B

Martensitic transformations: first-principles calculations combined with molecular-dynamics simulations*

P. Entel[a], R. Meyer, K. Kadau, H.C. Herper, and E. Hoffmann

Theoretische Tieftemperaturphysik, Gerhard-Mercator-Universität Duisburg, 47048 Duisburg, Germany

Received: 3 February 1998 / Revised: 4 May 1998 / Accepted: 24 June 1998

Abstract. Results are presented of first-principles total-energy calculations and molecular-dynamics simulations of structural transformations in magnetic transition metal alloys like $Fe_{1-x}Ni_x$. While first-principles calculations allow to identify those structures having the lower total energy, molecular-dynamics simulations can be used to trace out the dependence of the transformation on temperature, composition, concentration of defects *etc.* We have used the method of the semi-empiric embedded-atom potential in the molecular-dynamics simulations which yields remarkable good results for the structural changes.

PACS. 75.50.Bb Fe and its alloys – 81.30.Kf Martensitic transformations – 02.70.Ns Molecular dynamics and particle methods

1 Introduction

Research on martensitic phase transformations [1] in ferrous alloys covers a period of more than 100 years and has led to some understanding of the kinetics of the transformation (for a recent review see [2]). Martensitic transformations occur in alloys of different metallic elements. Usually the alloys are substitutional mixtures, where atoms of the host element are partially replaced by different kinds of metal atoms. This can lead to reduced or extra electronic charge. In the Hume-Rothery alloys this is responsible for the appearance of a definite crystal structure if the ratio of the valence electron number to atom number gets a certain value. But band filling, screening and atomic disorder effects connected with the extra charges do not only lead to martensitic transitions: They are responsible for a whole class of phenomena like precipitation, spinodal decomposition (and ordering) and other phase separation phenomena. The task of theory is to give a unified description of the electronic origin. In spite of many systematic theoretical investigations (for example, see [3]) this problem has not been completely solved. In this article we try to address a few fundamental questions associated with martensitic transformations in ferrous alloys with the help of first-principles calculations combined with molecular-dynamics simulations.

The martensitic phase transformation and structural trends of Hume-Rothery alloys are rather well understood. They are driven by the van Hove singularities in the density of states arising from band gaps at specific Brillouin zone boundaries. Is the new crystal structure for a critical electron number so that the new Brillouin zone can accommodate all electrons, a large energy gain can be expected. However, detailed calculations show that in addition the renormalization of electronic properties due to the logarithmic singularity in the slope of the Lindhard function at $q = 2\,k_F$ is important. Since this singularity is driven by the ratio of valence electron number to atom number, the Hume-Rothery alloys are called *electron phases*. In Hume-Rothery alloys the phase transition is of weakly first order from a high-temperature less-close packed structure to a low-temperature close-packed one.

The hysteresis associated with the transformation and the influence of atomic disorder or lattice defects on the width of the hysteresis are less well understood. Systematic first-principles investigations have shown that in many Hume-Rothery alloys compositional short-range ordering occurs which is again related to details of the Fermi surface touching the Brillouin zone. This determines the behavior of the atomic pair correlation function in an essential way [4,5]. Atomic ordering effects seem also to be important for the shape-memory alloys which usually show stoichiometric order, and for metals showing rubber-like behavior [6]. Rubber-like behavior seems to be caused by atomic short-range ordering of atoms or vacancies (aging process) leading to superelastic behavior.

There is some qualitative understanding but no microscopic theory of kinetic details of the martensitic transformation like nucleation of martensite at the surface or in the bulk at nucleation centers, concentration of martensitic embryos in the melt, role of diffusion processes *via* vacancies *etc.*

Structural transformations in ferrous alloys, where magnetic long-range order and spin fluctuations interfere, are less well understood. The experimental observation

* Dedicated to J. Zittartz on the occasion of his 60th birthday

[a] e-mail: entel@thp.uni-duisburg.de

is that in alloys with a ferromagnetic ground state, the less-close packed crystal structure can be stabilized at low temperatures. Hysteresis, supercooling, and superheating effects are usually more pronounced in the magnetic alloys. There are only a few stoichiometrically ordered phases. The element iron itself is interesting, since it can exist as bcc (α, δ), fcc (γ) or hcp (ε) phase. Iron-based alloys including Fe-C, Fe-Ni, Fe-Mn *etc.* usually exhibit the same richness of phases but also show systematic changes due to changes in the valence-electron number. *Ab initio* calculations of the total energy and magnetic moments of the bcc, fcc and hcp phase of iron as a function of volume explain the ferromagnetic bcc $\rightarrow$ paramagnetic hcp transition around 10 GPa. Under pressure the d band widens and the density of states at the Fermi energy ε_F decreases until the Stoner criterion for ferromagnetism is no longer fulfilled [7]. There is also a very strong volume dependence of the fcc and hcp moments near the normal atomic volume. The stability of the bcc structure at low temperatures is due to long-range ferromagnetic order.

The physical picture at finite temperatures is less clear. It has been argued very early that the occurrence of the γ-phase at higher temperatures is driven by large ferromagnetic spin fluctuations as first assumed by Weiss [8]. Interpretation of the behavior of the specific heat of the α- and γ-phase leads to the same conclusion [9]. At still higher temperatures the return to the bcc-like δ-phase is assumed to arise from entropy contributions of the softer δ-phase phonons or from loss of magnetic short-range order with increasing temperature [10]. The assumption of a magnetically driven $\alpha \rightarrow \gamma$ transition with increasing temperature has recently been questioned [11]. Investigation of the phonon dispersion of α-Fe reveals strong softening of the entire $T_1[\xi\xi 0]$ and $T_1[\xi\xi 2\xi]$ branch when approaching the $\alpha \rightarrow \gamma$ transition. The eigenvectors of these phonons are in the direction of displacements needed for the γ-phase. This has been interpreted by the authors as a dynamical precursor for the martensitic transformation. The data also suggest that the high-temperature phase is mainly stabilized by the increase in vibrational entropy, the entropy difference being $\Delta S^{\alpha\gamma}_{vib} = 0.142$ k_B/atom $= 0.887\times10^{-3}$ mRy/atom K or $T\Delta S^{\alpha\gamma}_{vib} = 1.05$ mRy/atom at $T = A_3 = 1184$ K which is larger than the value extrapolated from [9] giving $T\Delta S^{\alpha\gamma}_{vib/mag} = 0.606$ mRy/atom. Thus the controversy of what stabilizes the high-temperature γ-phase of elemental iron needs further inspection. The transition is not completely driven by the entropy of ferromagnetic spin fluctuations alone; the vibronic part of the entropy might be of equal importance which would confirm the conjecture of Petry [11].

Further problems arise when we try to describe the martensitic transformation on a microscopic level. While first-principles total-energy calculations give reliable results for the energy difference between different crystal structures at zero temperature for elemental iron and Fe-Ni alloys [12–14] or alkali elements [15,16]), and also allow to simulate the structural transformation from the $\gamma \rightarrow \alpha$ structure along the Bain path [17], the continuation to finite temperatures in form of first-principles molecular-dynamics simulations is still restricted to so small numbers of atoms that structural changes can not be simulated.

Also unsolved is the question of how to incorporate magnetism at finite temperatures. Therefore, in the present work we have combined first-principles total-energy calculations and semi-empiric molecular dynamics simulations based on the embedded atom method introduced by Daw and Baskes [18]. The latter method allows to handle a sufficiently large number of atoms and to simulate premartensitic behavior and the martensitic transformation [19–22].

Magnetism can be indirectly dealt with by using potential functions which reproduce the correct elastic behavior of the magnetic alloys at low temperatures. The simulations then allow to study the growth of martensite, for example, in thin Fe-Ni films with notch-like defects which facilitate martensitic nucleation at the surface [23]. In this paper we will discuss a few characteristic results for ferromagnetic and antiferromagnetic Fe and Fe-Ni alloys and nonmagnetic Ni-Al alloys.

2 Results of first-principles total-energy calculations

We first discuss results for elemental α- and γ-iron. Results of first-principles calculations of the total energy of the ferromagnetic (FM) and antiferromagnetic (AF) phase as function of the volume per atom are shown in Figure 1. The results differ from results of previous calculations with non full-potential methods [25] as discussed in [26]. The calculations were done by using the full-potential WIEN95 code [24]. In all calculations the scalar relativistic version and the generalized gradient approximation (GGA II) was used. The k-mesh used corresponds to 250 k-points in the irreducible wedge in the case of bcc Fe, to 145 k-points in the case of FM fcc Fe, to 150 k-pints in the case of hcp Fe, and to 315 k-points in the case of AF fcc Fe. The radius of the muffin-tin sphere was consistently chosen to be 2.2 a.u. Inside the muffin-tin sphere potential and charge density were expanded up to $L = 6$. For the interstitial region we have used a plane-wave cut-off of $R_{mt} \times K_{max} = 9.0$ which has proved to be accurate enough for d-orbitals. The equilibrium volumes were obtained from fits to Murnaghan's equation of state. In the case of AF order we considered only the AF I structure which consists of alternating layers of up and down spins.

Figure 1 shows that (i) FM α-Fe has the lowest ground-state energy, (ii) next lowest in energy would be nonmagnetic (NM) hcp Fe, (iii) γ-Fe would be AF but with close in energy lying FM low-moment state (at low volume) and high-moment state (at high volume) as well as many non-collinear states which have been omitted from Figure 1. There is also a tendency of γ-Fe to form a spin glass. This competition of many different magnetic states in γ-Fe is due to the behavior of the exchange integral which is small and has contributions with oscillating sign from many neighbor shells (kind of RKKY-like interaction mediated by the s and p electrons). These findings agree with

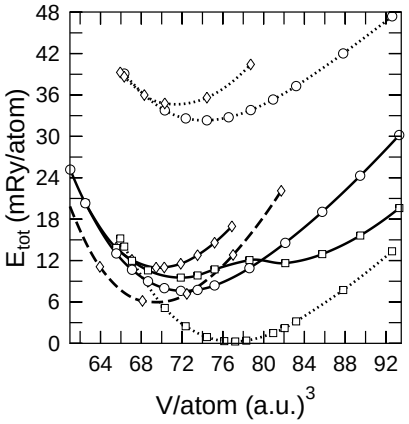

Fig. 1. Total energy of bcc, fcc and hcp iron as function of the atomic volume relative to the ground state energy of ferromagnetic bcc iron. Dotted curves refer to the bcc phase, solid curves to the fcc phase and the dashed curve to the hcp phase. Squares denote FM, circles antiferromagnetic (AF I), and diamonds nonmagnetic solutions.

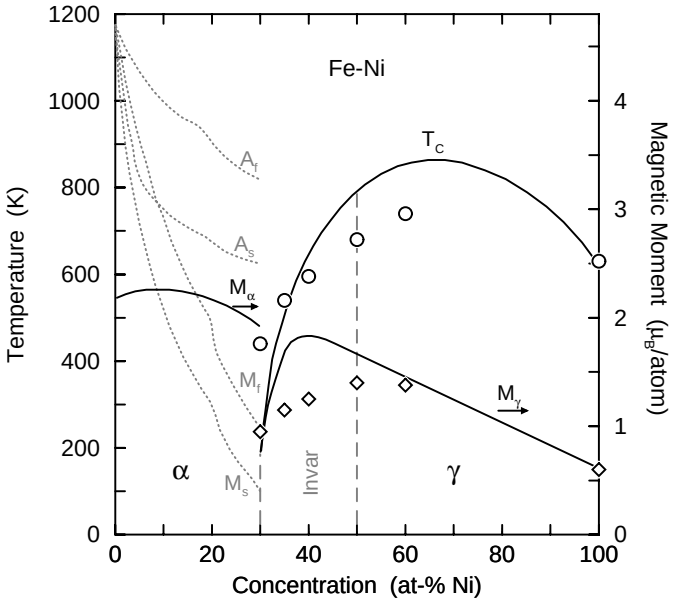

Fig. 2. Calculated Curie temperatures and magnetic moments per atom (circles and diamonds, respectively) of $Fe_{1-x}Ni_x$ in comparison with experimental data (solid lines). M_s, M_f, A_s and A_f are start and final temperatures of the martensitic and austenitic transformation. Also shown are the stability ranges of the bcc and fcc structure and the Invar region.

experimental data and the complex phase diagram of Fe-Mn and Fe-Ni (see Fig. 2) alloys on the Fe-rich side. The question is whether we can draw some reliable conclusions from the zero-temperature calculations about the magnetic behavior and structural $\alpha \rightarrow \gamma$ and subsequent $\gamma \rightarrow \delta$ transformation at high temperatures. This is indeed possible if we analyse total energies not only as a function of the volume per atom but also as a function of the magnetic moment per atom. This leads to magnetic binding surfaces usually evaluated by the fixed-spin moment method. This is a very time consuming calculation if we use the

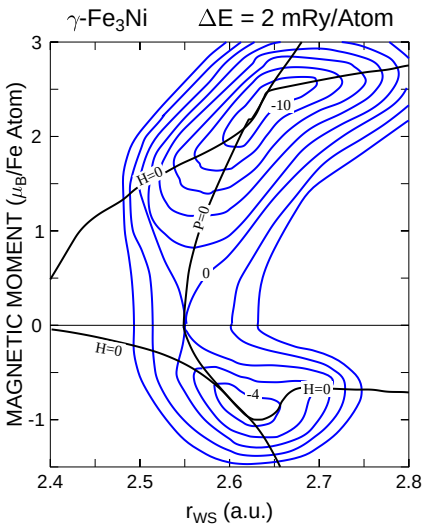

Fig. 3. Binding surface of Fe_3Ni as obtained from total energy FLAPW calculations. Contour lines are at 2 mRy/atom intervals. The ground state is FM separated from the NM saddle point by 10 mRy and from the AF minimum by 6 mRy (the lower part with negative moments is the AF region). Also shown are the $H = (\partial E/\partial M)_V = 0$ and $P = -(\partial E/\partial V)_M = 0$ lines.

full-potential method. Therefore, we have used the data in Figure 1 and corresponding data for Fe_3Ni to extract the surfaces. This is possible because the data in Figure 1 correspond to energies on the $H = (\partial E/\partial M)_V = 0$ line, where H is a ficticious external field which allows to fix the magnetic moment per atom. For briefness we omit the corresponding binding surface of γ-Fe and present results only for γ-Fe_3Ni which is of special interest because of the interference of magnetic and structural phase transitions and Invar anomalies.

Figure 3 shows that the ground state of γ-Fe_3Ni is FM lying 6 mRy (1 mRy $\approx$ 158 K) below the AF minimum. But let us first discuss the corresponding surface of γ-Fe which is slightly different from Figure 3. Here it is the AF state which is lowest in energy being separated by a few mRy from the shallow local FM minima corresponding to a low moment at low atomic volume and a high moment at a larger volume in agreement with the data in Figure 1. This also agrees with the experimental observation that γ-Fe has an AF ground state at appropriate lattice spacing [27,28].

Corresponding energy surfaces for γ-Fe and γ-Fe_3Ni can also be evaluated at finite temperatures by retaining fluctuations in Gaussian approximation [29–32]. For example, this allows to speculate about the finite-temperature behavior of γ-Fe: The AF solution will gradually disappear with increasing temperature, leaving at higher temperatures dominating FM spin fluctuations which lead to an enhanced atomic volume and anti-Invar behavior. These FM spin fluctuations are easy to excite and do not cost much energy. The spin fluctuations (in addition to the lattice vibrations) will also help to stabilize the γ-phase with respect to the α-phase at elevated temperatures in

the absence of long-range FM order in accordance with the $\alpha \rightarrow \gamma$ phase transformation with increasing temperature in elemental Fe. This scenario is in agreement with Hasegawa's model calculation of the phase diagram of iron [10].

We can also model this $\alpha \rightarrow \gamma$ transition at zero temperature by using *ab initio* calculations. They show that the transition is associated with a substantial charge transfer from t_{2g} orbitals to e_g orbitals. The consequences of such a charge transfer would result in a lower atomic volume right after the transition in the γ-phase. This is indeed observed in experiments. This kind of charge transfer also occurs in the Fe-Ni alloys and is responsible for the Invar anomalies [33].

When discussing alloy systems, it is important to know whether they have more or less valence electrons than elemental iron. Adding extra d electrons like in the Fe-Ni Invar alloys destabilizes the bcc structure leading to Invar behavior in the γ-phase. This instability has two aspects, one is associated with the extra charge [33], the other with lattice vibrational arguments (for example, in bcc Ni the shear modes have negative squared phonon energies [21] which also helps to destabilize the low-temperature α-phase of the FeNi alloys).

We now discuss the binding surface of Fe_3Ni in Figure 3 (obtained from the data set in Ref. [34]). There still is an AF solution, but it is now the FM state which is more stable. Due to the specific form of the surface, we expect strong admixture of FM and AF spin fluctuations at temperatures lower than the Curie temperature. Atomic disorder will further contribute to competing spin fluctuations. The Invar instability itself is related to these fluctuations which couple strongly to phonons and local $e_g \rightleftharpoons t_{2g}$ charge fluctuations [33]. Because of the specific form of the surface, we expect that FM spin fluctuations will dominate at temperatures higher than the Curie temperature T_c in much the same way as in γ-iron. In this way we can explain Invar-like behavior for $T < T_c$ and anti-Invar behavior for $T > T_c$ in the Fe-Ni alloys.

When the number of d electrons is reduced like in the Fe-Mn alloys, the ground state of the γ-phase becomes AF leading to anti-Invar behavior above the Néel temperature as in the case of γ-iron. Both alloy systems, Fe-Ni as well as Fe-Mn, are disordered and have lower martensitic transition temperatures than elemental iron. The transition temperature decreases further with increasing concentration of Ni or Mn atoms.

The strong concentration dependence of the martensitic transition temperature is a longstanding problem. Figure 2 shows the strong variation of the martensitic and austenitic transition temperatures with concentration for the Fe-Ni system. Also large supercooling and superheating effects can be observed. It has recently been argued that the large dependence on concentration could be associated with strong mass-disorder scattering of phonons [35] which, however, in the case of Fe-Ni might be doubtful since Fe and Ni have practically the same atomic mass. Disorder scattering occurs here in the minority-spin channel because the energies of the 3d-minority-spin states of Fe and Ni are different. This leads to strong disorder effects in the minority-spin density of states curve. In order to gain more insight into the dependence on concentration, we have performed first-principles total-energy calculations by using the KKR-CPA method for the disordered alloys [14]. In addition the FLAPW/GGAII method has been used to calculate energy differences for a few stoichiometric cases. The resulting dependence of energy differences on concentration agrees qualitatively with the behavior of transition temperatures for the structural transformation in Figure 2. This is remarkable, since it proves that the strong variation, for example, of M_0 (which is the thermal equilibrium martensitic transition temperature, where the free energies of the α- and γ-phase cross) with concentration is an intrinsic effect and associated with the concentration dependence of the energy barrier between the α- and γ-phase. This energy difference is gained by martensitic nucleation in parent austenite, whereby the gain in energy has to overcome the energy cost associated with increasing stress during the growth of the nucleus. This partially solves the longstanding problem of what determines the concentration dependence of the martensitic transition temperature in ferrous alloys.

The remaining question to be answered is, what is responsible for the strong concentration dependence of the energy difference between the α- and γ-phase? This brings us back to the observation that it is FM order which stabilizes the bcc structure at low temperatures. First-principles calculations for α-Fe and Fe-Ni actually prove that it is the magnetic contribution to the energy which stabilizes the less-close packed bcc structure at zero temperature [14]. At high temperatures this is no longer evident as discussed in the introduction. We thus face the interesting situation that we can have different stabilizing mechanisms acting at different temperatures in the Fe-Ni alloy system: At low T it is the magnetic pressure which stabilizes the bcc structure; at high T it is the vibrational entropy and strong FM spin fluctuations which stabilize the fcc structure.

The origin of the strong concentration dependence of the energy difference between the fcc and bcc structure is at low temperatures connected with a subtle interplay of different magnetic ordering tendencies and related occupation of antibonding and nonbonding d-orbitals. This brings us back to the binding surfaces discussed before. Adding Ni to FM α-Fe which has large exchange splitting between minority-spin and majority-spin states, destabilizes the bcc structure because extra d-electrons from Ni mainly go to the nonbonding states. This leads to reduced partial electronic pressure, to a decrease of the volume, and finally to FM order in the fcc structure at still higher concentrations of Ni. At finite temperatures the contributions of phonons to the entropy can not be neglected and might be of the order of the magnetic contribution.

The forestanding discussion shows that the change of electronic properties with Ni concentration in the Fe matrix plays an important role. However, is this sufficient to explain the martensitic transformation? At finite temperatures the coupling of electrons to phonons

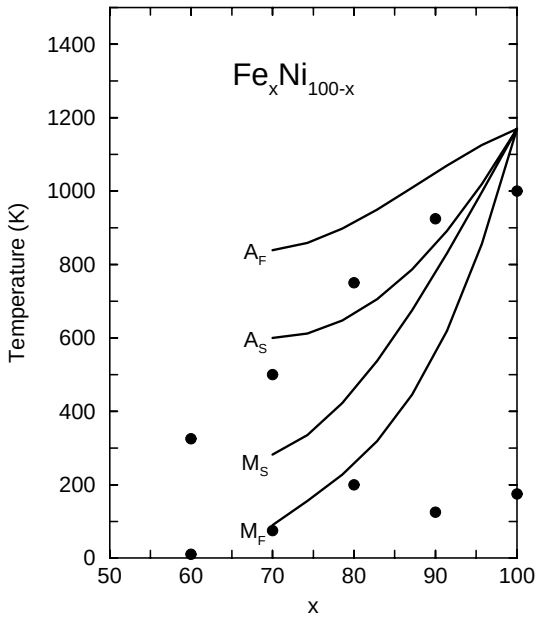

Fig. 4. Phase diagram of Fe-Ni as obtained by molecular-dynamics simulations: Upper dots for the $\alpha \rightarrow \gamma$ transition with increasing temperatures and lower dots for the $\gamma \rightarrow \alpha$ transition with decreasing temperatures. Solid lines are experimental data for $A_{s,f}$ and $M_{s,f}$.

and resulting phonon softening due to Fermi-surface nesting will help to induce a structural transformation in the Fe-Ni alloys [13,14,26,34,36–38]. Of special interest is in this case the interplay of magnetic order. Evaluation of electron-phonon matrix elements show that it is mainly the coupling of minority-spin electrons to phonons which is responsible for phonon softening effects going hand in hand with the decrease of the minority-spin density of states at the Fermi energy while passing from the fcc to bcc structure along the Bain path. This leads in the bcc structure of Fe-Ni alloys to remarkable softening of the $T_1[110]$ phonon with increasing temperature as observed in the molecular-dynamics simulations [21]. The softening is most pronounced at the zone boundary and at the temperature, where the simulations show a sudden transition from bcc to fcc. However, the phonon does not completely soften at the transition. This agrees with the behavior of the corresponding phonon in α-Fe as observed by neutron scattering [11]. Similar discussion of Fermi-surface nesting and softening of transverse phonons as dynamical precursor of the austenitic or martensitic transformation in Ni-Ti and Ni-Al can be found in [39–41].

Another problem is connected with hysteresis effects which are difficult to deal with in the *ab initio* calculations. It is known that the transformation starts with the formation of lenticular or needle-like nuclei of martensite around defects in the parent phase. These nuclei usually grow in size into *easy directions* until they meet other martensitic grains. The magnitude of supercooling, superheating and hysteresis effects is usually attributed to the degree of difficulty of the system to accommodate the continuous nucleation production and the difference of shape between the two phases. It is out of scope of the present work to discuss in detail the different contributions to the free energy in the two phases due to growing martensitic or austenitic palets. However, molecular-dynamics simulations of the transition in Fe-Ni in the presence of impurities (vacancies) discussed below, show that the temperature range of supercooling and superheating is not arbitrary or a complex function of the concentration of various lattice defects, but is characteristic for the specific alloy under consideration [23,38]. Also the hysteresis depends strongly on the energy difference between the fcc and bcc structure. Defects will further broaden the transition; but they are not originally responsible for the structural transformation as a phase transition of first order.

3 Results of molecular-dynamics simulations

With increasing computer power molecular-dynamics simulations have become a standard method of statistical mechanics. For example, they have been used successfully in investigations of dynamical properties, spinodal decomposition and pattern formation of mixtures of liquids. The low density of fluids allows to cover a time scale which is sufficient for the evaluation of the time dependence of the velocity-velocity correlation function. Integration over time then yields reliable values for diffusion constants. Even growth exponents can be predicted which agree with experiment. Similar simulations in solids give much less information since simulation times are restricted to reciprocals of typical phonon frequencies. This means that segregation effects like spinodal decomposition have not yet been simulated successfully. Therefore, it is remarkable that transformations of solids bearing traces of spinodal decomposition like the martensitic transformation, can be investigated with the help of molecular-dynamics simulations. In contrast to liquids, where simple Lennard-Jones potentials yield accurate results, it is important that one uses more refined many-body interatomic potentials for the solids. Here the embedded-atom method [18] has been used with success to construct the potentials.

Simulation of the martensitic transformation at finite temperatures is possible by using a thermostat [42] and a fluctuating volume box [43]. So different crystallographic structures can be simulated by using the same N-body interatomic potential in the different phases. In the following we will discuss a few aspects connected with molecular-dynamics simulations of the austenitic and martensitic transformation in Fe-Ni and Ni-Al alloys. Figure 4 shows results of simulations of the phase diagram of Fe-Ni. There is some disagreement with the experimental phase diagram on the Fe-rich side because magnetism is not taken into account in an optimal way in the simulations. But supercooling and superheating effects are clearly visible.

It is of interest to discuss briefly molecular dynamics simulations of martensitic transitions in other alloy systems. Analysis of the structural transition in Ni-Al [44,45] has shown that the transition is first order, entropy driven, and follows the *Zener picture* [46] according to which the

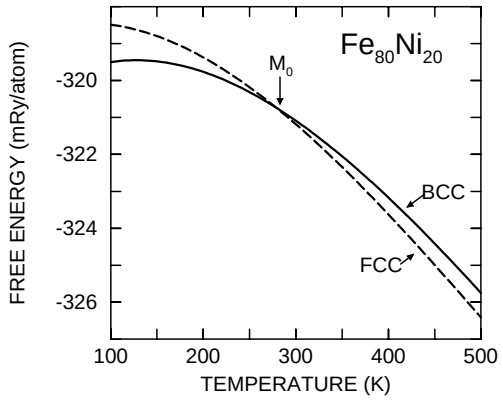

Fig. 5. Free energy as a function of temperature for α- and γ-$Fe_{80}Ni_{20}$ as obtained by molecular-dynamics simulations. The crossing of the free energies defines M_0.

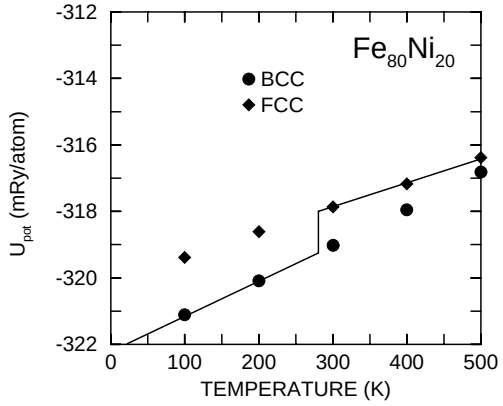

Fig. 6. Potential energy as a function of temperature of $Fe_{80}Ni_{20}$ as obtained by molecular-dynamics simulations.

transformation is due to the competition of internal energy and entropy between the austenitic and martensitic phase. Entropy driven means that it is the higher vibrational entropy of the austenitic phase which is responsible for the transition when increasing the temperature with a considerable increase of the mean square displacement of the atoms in the high-temperature phase. For example, the entropy change for the composition $Ni_{64}Al_{36}$ is $T\Delta S = 0.26$ mRy/atom at the transition. With respect to disorder, the entropy differences between different atomic configurations are very small in the Ni-Al alloys. Therefore, the hypothetical equilibrium martensitic transformation temperature of the Ni-Al alloys, M_0, follows the difference of the (internal) energy of the various atomic configurations [44]. This allowed to describe the influence of disorder on the martensitic transformation temperature in a coherent way.

It is interesting to check whether this kind of picture for the Ni-Al alloys is also valid in the case of magnetic alloys. If we assume that for small changes in concentration the entropy differences between the fcc and bcc phase will not drastically change, then $M_0(x)$ should scale

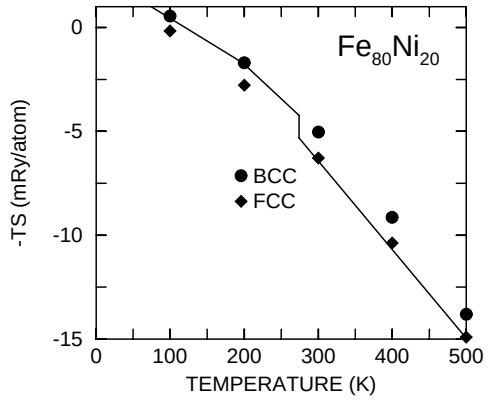

Fig. 7. Entropy as a function of temperature of $Fe_{80}Ni_{20}$ as obtained by molecular-dynamics simulations.

with $|E_{fcc} - E_{bcc}|(M_0, x) \sim M_0(x)$. The calculations show that corresponding energy differences in Fe-Ni evaluated at zero temperature, indeed scale with $M_0(x)$, although we do not know the experimental $M_0(x)$ exactly.

We now discuss results for the thermodynamic potential of Fe-Ni. The molecular dynamics simulations have been performed for the composition $Fe_{80}Ni_{20}$. Results for the free energy in Figure 5 show that the structural change is of first order. Results for the free energy of Ni-Al behave in much the same way [44]. The crossing of the free energies defines the equilibrium transition temperature M_0 which is different from $M_{s,f}$ and $A_{s,f}$ (martensitic and austenitic start and final temperatures, respectively).

We have already discussed experimental results for the entropy of elemental iron [9] which yield an entropy jump at A_3 of the order of 0.606 mRy/atom which must be compared with the vibrational value of 1.05 mRy/atom [11]. How does this value compare with results of molecular-dynamics simulations of Fe-Ni alloys? Figures 6 and 7 show results for the temperature variation of the potential energy and the entropy of $Fe_{80}Ni_{20}$, respectively (the kinetic energy has been subtracted since it is the same in both phases). As in the case of Ni-Al, the variation of TS is much larger than the variation of the potential energy which is a hint that the transition is driven by the entropy. The magnitude of the entropy change at M_0 is of the order of $T\Delta S = 1$ mRy/atom. Although the transition temperature M_0 is much smaller than A_3 of elemental Fe, the value for the entropy change agrees remarkably well with the experimental value given in reference [11] and less well with the value obtained from the specific heat data which is smaller. The entropy change in the simulations is mostly of vibrational origin. A magnetic part can not be split off, since magnetism enters the simulations only by fitting the embedded-atom potentials used in the simulations so that the elastic properties of the bcc phase is in agreement with experimental data. However, we may conclude that both, vibronic and magnetic contributions to the free energy will be important and determine the martensitic transition at A_3 in elemental Fe and in the Fe-Ni alloys, *i.e.* the vibrational excess entropy of the fcc structure due to large mean

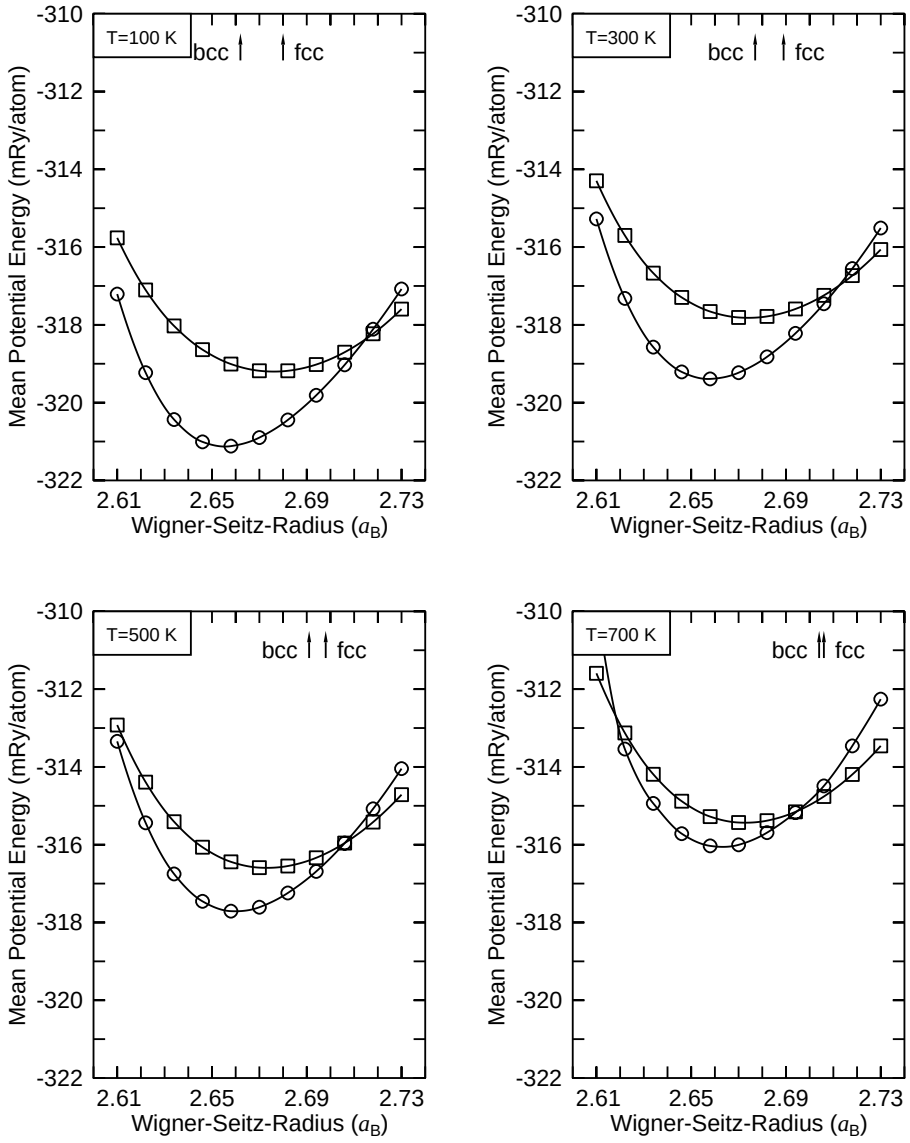

Fig. 8. Mean potential energy of $Fe_{80}Ni_{20}$ for the bcc and fcc structure as a function of the Wigner-Seitz radius at different temperatures. The Wigner-Seitz radius at equilibrium is marked for each structure by arrows. The equilibrium does not coincide with the minimum of the individual energy curve, since due to the missing entropy, the energy does not correspond to the free energy. The bcc structure is marked by circles, the fcc structure by squares. With increasing energy the difference in potential energy between fcc and bcc structure decreases until they approximately coincide at the structural transition ($\approx$ 700 K).

square amplitudes of the atomic vibrations is at least as important as the magnetic excess entropy due to strong FM spin fluctuations with large mean square amplitudes. For a discussion which emphasizes more the importance of magnetic fluctuations see [47].

Finally we would like to show, how the structural transformation is achieved in the molecular dynamics simulations. This can be done by inspecting the behavior of the volume dependence of the free energy as a function of temperature and by following on a microscopic level the creation of twin boundaries and stacking faults due to the structural transformation. Since the evaluation of the entropy is very time-consuming in the simulations, only results for the potential energy are shown in Figure 8. In order to obtain these results, simulations had to be carried out in the (N, V, T) ensemble (constant particle number, volume and temperature) while simulations for the structural transformation must be done in the (N, P, T) ensemble. Figure 8 shows that the structural transformation from $\alpha \rightarrow \gamma$ at $A_s \approx 700$ K occurs at a volume for which the potential energy of the fcc phase is lower than in the bcc phase. So it is finally the energy barrier of the potential energy which must be overcome, although the transition is driven by the entropy.

Along with the structural transformation from bcc to fcc in the Fe-Ni alloys upon heating, twin boundaries and stacking faults are created. Figure 9 shows results for the $Fe_{65}Ni_{35}$ alloy. The following orientational relationships

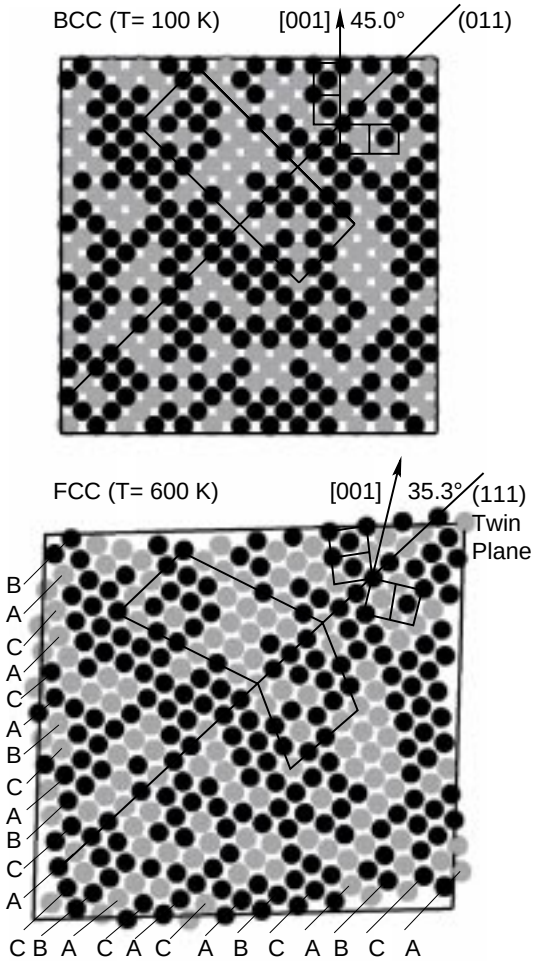

Fig. 9. Transformation of the bcc structure of $Fe_{65}Ni_{35}$ (upper panel) to the fcc structure (lower panel) by forming twins and stacking faults. Fe atoms are black, Ni atoms are grey. Paper plane is (100) for bcc and $(1\bar{1}0)$ for fcc, respectively.

can be observed: $(011)_{bcc} \approx (111)_{fcc}$, $[001]_{bcc} - [001]_{fcc} \approx 9°$ being close to experimental values. A detailed analysis of the influence of different kinds of defects on the transformation and growth processes of embryos and final nucleation is under current investigation. Although at present defects are limited to vacancies, free surfaces and surfaces with big notch-like defects, there are promising results for growth processes of martensite under the influence of these defects and under the influence of additional external strain. For example, investigations have been done with respect to superelastic behavior of thin Fe-Ni films and shape-memory effects in Fe-Ni bulk systems [38]. Here we cite the main results. Thin Fe-Ni films with composition $Fe_{70}Ni_{30}$ have initially been prepared in the fcc structure at low temperatures. In order to facilitate the nucleation of martensite, a large notch-like defect has been prepared in the film plane. After thermalizing tensile stress has been applied, leading to 6% expansion of the film and the appearance of typical martensitic texture which gradually disappears if external forces are swichted off and the system is allowed to relax. Elemental Ni, for example, behaves completely different in the simulations. Here we observe fracture when tensile stress is applied, with a crossover from brittle fracture at low temperatures to ductile fracture as plastic shear with emission of dislocations at high temperatures, in agreement with experiment. This proves that (apart from the poor treatment of magnetism) the embedded atom potentials used for the description of the Fe-Ni alloys are very accurate. One-way shape memory effects have also been observed during the simulations [38]. If we heat $Fe_{80}Ni_{20}$ in the simulations up to 700 K, the alloy transforms to the fcc structure. We then stress the system at 800 K till an expansion of 12% is reached. By switching off the load and subsequent cooling down to 200 K, the system gains back its original bcc structure practically without formation of additional defect structures. However, in order to achieve this, a very high concentration of vacancies of the order of 2% is needed. Here further simulations are needed in order to clarify the shape memory effect in relation to defects at fixed positions required for nucleation of martensite at always the same local sites.

4 Summary

In this paper we have shown that *ab initio* full-potential calculations and *semi-empiric* molecular-dynamics simulations can be used to clarify various aspects of martensitic transformations. The *ab initio* calculations have shown that magnetic order is able to stabilize less-close packed crystal structures at low temperatures like α-iron. Iron alloys in the close-packed fcc or hcp structure are of special interest because of competing magnetic interactions. In particular the Invar effect is related to these competing interactions. Its origin can be traced back to charge transfer effects between orbitals of different spin and different bonding character. The stabilizing effect due to magnetic order becomes less effective at high temperatures because of the growing influence of vibrational entropy. Here molecular-dynamics simulations are an appropriate tool to obtain information about the structural transformation and the temperature variation of thermodynamic potentials.

Appendix

We give here a brief account of some details related to the molecular-dynamics simulations. We used the embedded-atom method, where the total energy is written as the sum of an embedding function and a screened Coulomb potential,

$$E_{total} = \sum_i F_i(\rho_i) + \frac{1}{2}\sum_i \sum_{j \neq i} \phi_{ij}(r_{ij}) \qquad (1)$$

with $r_{ij} = |\mathbf{r}_i - \mathbf{r}_j|$. The index i stands for the lattice site and the kind of atom at that site. We have used the procedure of Daw and Baskes [18] which consists of constructing the electronic charge density of the solid at site i from

spherical symmetric charge densities of the surrounding atoms $\rho_i = \sum_{j \neq i} \rho_{at,j}(r_{ij})$. For details of obtaining $\rho_{at,j}$ from orbitals of valence electrons of free atoms see reference [18]. The function $\phi_{ij}(r)$ is given by $2Z_i(r)Z_j(r)/r$ (the factor 2 is due to using Bohr' radius a_0, elementary charge e and Rydberg for measuring distance, charge and energy). The embedding functions $F_i = F_{\mathrm{Fe}}$, F_{Ni} and the effective charges $Z_i = Z_{\mathrm{Fe}}$, Z_{Ni} are cubic spline functions. The parameters of these functions have been obtained by a fit to experimental data of the lattice constants, sublimation energies, elastic constants C_{11}, C_{12}, and C_{44}, vacancy formation energies, and some selected phonon frequencies of pure Fe and Ni. The parameters including their derivatives can be found in reference [21] and will not be listed here again. Magnetism is accounted for only in so far as the fit is made to experimental materials parameters of the pure elements Fe and Ni at low temperatures.

Standard molecular-dynamics simulations were then performed employing the verlet velocity algorithm with a time step of 1.5 fs and periodic boundary conditions. In the simulations of $Fe_{65}Ni_{35}$, the initial configuration consists of 4394 atoms, arranged on an ideal lattice of $13 \times 13 \times 13$ bcc cells. Several such configurations were prepared in order to test the influence of different atomic disorder on the austenitic transformation. With these configurations, simulations were done in the (N, P, T) ensemble generated by the Nosé-Hoover thermostat method [42] combined with the Parrinello-Rahman scheme [43]. Upon heating the bcc structure transforms to the austenitic fcc structure with formation of twin boundaries and stacking faults as shown in Figure 9. At each temperature a sufficient number if MD steps (500–1000) has been performed to allow the system to relax. The transformed lattice shown in Figure 9 is not an instant snap shot. Since the atoms move during the simulation, an average has to be taken over many simulation steps (5000) at one and the same temperature. This averaging eliminates to some degree the displacements from ideal fcc lattice positions. Also atoms in Figure 9 are not the same size (the size of the atoms in Fig. 9 is only guide to the eyes). The type of crystal structure in the simulations is obtained from a calculation of the atomic pair distribution function.

The calculation of free energies of alloys from the MD simulations is problematic, since integration over small portions of the internal energy has proven to be not a useful tool due to the oscillatory behavior of E in the simulations. One way to evaluate free energies is to introduce an effective Hamiltonian $H_{eff}(\lambda) = (1-\lambda)H_0 + \lambda H_1 = H_0 + \lambda \Delta H$, where H_0 is the Hamiltonian of the actual system and H_1 corresponds to the reference system. The free energy difference can then be obtained by the thermodynamic path which connects both systems,

$$\Delta F = \int_0^1 d\lambda \frac{\partial H_{eff}(\lambda)}{\partial \lambda}. \qquad (2)$$

This method has recently been used to evaluate the free energy of the different phases of Sn [48], whereby the integral was computed as time average over a time interval much longer than the vibrational period. This requires many MD simulations. The method can also be used to discuss the vibrational entropy differences between ordered and disordered structures like, for example, in Ni_3Al [49]. Another method, which has recently been applied to Ni_3Al, is to use the quasi-harmonic approximation for the free energy [50].

We have used a method, where an approximate free energy can be obtained from a single MD simulation [51]. This is possible if the variational principle of the free energy $F \leq F_0 + \langle V - V_0 \rangle_0$ is used, where the average is with respect to a trial potential V_0 with a known free energy F_0. This can be used to obtain the entropy in the form $S \leq S_0$ with $S_0 \propto \ln(\det C)$, where $C_{ij} = \langle x_i x_j \rangle - \langle x_i \rangle \langle x_j \rangle$ is the correlation matrix $(i, j = 1 \ldots 3N)$. Both methods have their disadvantages. The former method requires an assumption of how λ varies with time; the latter method requires the evaluation of the correlation matrix and one does not really know how big the error is. The equilibrium transition temperature M_0 obtained by the approximative method (by comparing the free energies of the bcc and fcc phase, see Fig. 5) must lie between the actual transition temperature for the austenitic and martensitic transformation in Figure 4. This is fulfilled. Therefore, we anticipate that the approximative method gives some reliable information about the entropy for each crystal structure and about the entropy difference between the two structures. A quantitative comparison of entropic contributions obtained with different methods in the MD simulations will be done in near future.

The configurational entropy has not been calculated. This should be done by using, for example, the cluster variation method, where combinatorics is used of arranging atoms on a crystal lattice, given a particular state of order. We have only checked that distributions of Fe and Ni atoms in the alloy, which for a given concentration are not too different from each other, do not affect the transformation temperature in a serious manner. The calculated internal energy depends of course on the configuration as well as the calculated vibrational entropies and vary with concentration.

This work was supported by the Sonderforschungsbereich 166 Duisburg-Bochum.

References

1. A. Martens, VDI-Zeitschrift **22**, 205, 483 (1878).
2. L. Delaey, in *Materials Science and Technology*, Vol. 5, edited by R.W. Cahn, P. Haasen, E.J. Kramer (Weinheim VCH 1991), p. 339.
3. D.G. Pettifor, in *Materials Science and Technology*, Vol. 1, edited by R.W. Cahn, P. Haasen, E.J. Kramer (Weinheim: VCH 1993), p. 61.
4. J.B. Staunton, D.D. Johnson, F.J. Pinski, Phys. Rev. B **50**, 1450 (1994).
5. J.D. Althoff, D.D. Johnson, F.J. Pinski, J.B. Staunton, Phys. Rev. B **53**, 10610 (1996).
6. R.W. Cahn, Nature **374**, 120 (1995).

7. J. Madsen, O.K. Anderson, U.K. Poulsen, O. Jepsen, in *Magnetism and Magnetic Materials*, AIP Conf. Proc. **29**, edited by J.J. Becker, G.H. Landes (New York: AIP 1976), p. 327.
8. R.J. Weiss, Proc. Phys. Soc. **82**, 281 (1963).
9. W. Bendick, W. Pepperhoff, Acta Metall. **30**, 679 (1982).
10. H. Hasegawa, D.C. Pettifor, Phys. Rev. Lett. **50**, 130 (1983).
11. J. Neuhaus, K. Nicolaus, W. Petry, B. Hennion, A. Krimmel, Physica B **234-236**, 897 (1997).
12. G.L. Krasko, G.B. Olson, Phys. Rev. B **40**, 11–536 (1989).
13. E. Hoffmann, H. Herper, P. Entel, S.G. Mishra, P. Mohn, K. Schwarz, Phys. Rev. B **47**, 5589 (1993).
14. M. Schröter, H. Ebert, H. Akai, P. Entel, E. Hoffmann, G.G. Reddy, Phys. Rev. B **52**, 188 (1995).
15. V.L. Sliwko, P. Mohn, K. Schwarz, P. Blaha, J. Phys.-Cond. Matter **8**, 799 (1996).
16. P. Mohn, K. Schwarz, P. Blaha, J. Phys.-Cond. Matter **8**, 817 (1996).
17. E.C. Bain, N.Y. Dunkirk, Trans. AIME **70**, 25 (1924).
18. M.S. Daw, M.I. Baskes, Phys. Rev. B **29**, 6443 (1984).
19. R. Meyer, P. Entel, J. Phys. IV Colloq. France **5**, C2-123 (1995).
20. R. Meyer, P. Entel, J. Phys. IV Colloq. France **7**, C5-29 (1997).
21. R. Meyer, P. Entel, Phys. Rev. B **57**, 5140 (1998).
22. R. Meyer, unpublished.
23. K. Kadau, P. Entel, R. Meyer, unpublished.
24. P. Blaha, K. Schwarz, P. Dufek, R. Augustyn, WIEN95, TU of Vienna 1995. Improved and updated UNIX version of the original WIEN-code, published by P. Blaha, K. Schwarz, P. Sorantin, S.B. Trickey, Comput. Phys. Commun. **59**, 399 (1990).
25. V.L. Moruzzi, P.M. Marcus, K. Schwarz, P. Mohn, Phys. Rev. B **34**, 1784 (1986).
26. H.C. Herper, E. Hoffmann, P. Entel, J. Phys. IV Colloq. France **7**, C5-71 (1997).
27. W.A.A. Macedo, W. Keune, Phys. Rev. Lett. **61**, 475 (1988).
28. A. Onodera, Y. Tsunoda, N. Kunitomi, O.A. Pringle, R.M. Nicklow, R. Moon, Phys. Rev. B **50**, 3532 (1994).
29. P. Entel, M. Schröter, Physica B **161**, 160 (1989).
30. D. Wagner, J. Phys.-Cond. Matter **1**, 4635 (1989).
31. M. Schröter, P. Entel, S.G. Mishra, J. Magn. Magn. Mater. **87**, 163 (1990).
32. P. Mohn, K. Schwarz, D. Wagner, Phys. Rev. B **43**, 3318 (1991).
33. P. Entel, E. Hoffmann, P. Mohn, K. Schwarz, V.L. Moruzzi, Phys. Rev. B **47**, 8706 (1993).
34. H.C. Herper, E. Hoffmann, P. Entel, in *Properties of Complex Inorganic Solids*, edited by A. Gonis, A. Meike, P.E.A. Turchi (New York Plenum 1997), p. 213.
35. P.A. Lindgard, J. Phys. IV Colloq. France **5**, C2-29 (1995).
36. H.C. Herper, P. Entel, W. Weber, J. Phys. IV Colloq. France **5**, C2-129 (1995).
37. H.C. Herper, E. Hoffmann, P. Entel, W. Weber, J. Phys. IV Colloq. France **5**, C8-293 (1995).
38. P. Entel, E. Hoffmann, M. Clossen, K. Kadau, M. Schröter, R. Meyer, H.C. Herper, M.S. Yang, in *The Invar Effect: A Centennial Symposium*, edited by J. Wittenauer (Warrendale: TMS 1997), p. 87.
39. G.L. Zhao, T.C. Leung, B.N. Harmon, M. Keil, M. Müllner, W. Weber, Phys. Rev. B **40**, 7999 (1989).
40. G.L. Zhao, B.N. Harmon, Phys. Rev. B **48**, 2031 (1993).
41. G.L. Zhao, B.N. Harmon, Phys. Rev. B **45**, 2918 (1992); Phys. Rev. B **47**, 8706 (1993).
42. S. Nosé, Molec. Phys. **50**, 1055 (1983).
43. M. Parrinello, A. Rahman, Phys. Rev. Lett. **45**, 1196 (1980).
44. S. Rubini, P. Ballone, Phys. Rev. B **48**, 99 (1995); Erratum: Phys. Rev. B **49**, 15 428 (1994).
45. S. Rubini, P. Ballone, Phys. Rev. B **50**, 1297 (1994).
46. C. Zener, Phys. Rev. B **71**, 846 (1947).
47. M. Acet, E.F. Wassermann, K. Anderson, A. Murani, O. Schärpff, J. Phys. IV Colloq. France **7**, C5-401 (1997).
48. R. Ravel, Phys. Rev. Lett. **79**, 2482 (1997).
49. R. Ravelo, J. Aguilar, M. Baskes, J.E. Angelo, B. Fultz, B.L. Holian, Phys. Rev. **57**, 862 (1998).
50. J.D. Althoff, D. Morgan, D. De Fontaine, M. Asta, S.M. Foiles, D.D. Johnson, Phys. Rev. B **56**, R5705 (1997).
51. J.R. Morris, K.M. Ho, Phys. Rev. Lett. **74**, 940 (1995).